(Received 3 January 2025, Accepted 13 February 2025, Scheduled 19 February 2025)

Polarization-Insensitive, Integrally Rectifying Metasurface Array for Ambient Energy Harvesting

Congcong Xia[1], Hongmei Zhao[1,*], Yunfei Wang[2], and Mingxing Ren[3]

[1] College of Electric and Information Engineering, Zhengzhou University of Light Industry, Zhengzhou, China
[2] Network Operations Division, China United Network Communications Corporation Limited, Beijing, China
[3] School of Information and Communication, Guilin University of Electronic Technology, Guilin, China

ABSTRACT: In this paper, an integrated rectifying metasurface harvester with small dimensions, wide-angle incidence, and polarization insensitive characteristics is proposed. The proposed structure is assembled from a periodic unit cell, diodes, and loads, which makes the structure simple and less expensive to manufacture. The centrosymmetric design concept of the unit cell structure enables the proposed metasurface harvester to capture incident waves with arbitrary polarization angles and over a wide incident angle range of 60°. A 5×5 metasurface array was fabricated for real measurements. The results show that the measured efficiency is 62.07% near the operating band 5.8 GHz when the incident power is 15 dBm. When the polarization angle of the incident wave is changed, the efficiency remains essentially constant. As the angle of incidence changes, the efficiency shows a certain decrease, but it can still maintain an efficiency close to 50% near the operating frequency band. The proposed harvester can supply energy to low power devices as well as sensor nodes in IoT.

1. INTRODUCTION

Nowadays, the advancements in Artificial Intelligence (AI) and 5G technology are propelling the Internet of Everything (IOE) to the forefront of technological trends. Across the globe, a vast array of low-power, compact smart terminal devices and wireless sensor nodes are being deployed, reaching every nook and cranny of the world [1–5]. The ability of these devices to work continuously in various complex environments for long periods of time has attracted much attention. Compared with the traditional manual battery replacement, which is used to increase the operating time of the devices, Ambient Energy Harvesting (AEH) allows devices to actively capture the electromagnetic energy present in the environment and convert the collected energy into direct current (DC) to power them [6]. The concept of electromagnetic metasurface (MS) was first proposed in [7], which consists of two-dimensional or quasi-two-dimensional sub-wavelength metamaterials in a planar surface arranged in a specific pattern. Metasurfaces' various unique properties, such as polarization rotational transformation and perfect absorption, have led to a wide range of applications in wireless energy transmission as well as energy harvesting, e.g., magnetically coupled systems [8, 9], medically implantable devices [10, 11], and rectifier antennas [12–14], among others.

Energy harvesting mostly uses a rectifier antenna as a harvester, which consists of a receiving antenna, a matching network, a rectifier circuit, and a load [15, 16]. In order to improve the energy harvesting efficiency, common strategies in current research encompass co-planar integration of the antenna with the rectifier circuit [17, 18], the use of metallized through-holes for energy pooling [19, 20], and multilayer coupling [21–23]. Co-planar integration of the antenna and rectifier is done by designing the energy transmission channel as the energy output port, which requires the design of a matching network along with limited design freedom [24, 25]. The use of metallized through-holes and multilayer coupling also requires the design of a matching network, which increases design complexity and manufacturing costs, which is not conducive to large-scale diffusion.

The input impedance of the rectifier circuit will mostly present a high impedance state, and metasurface antennas more readily exhibit high impedance characteristics than conventional antennas. Thus, eliminating the matching network through reasonable cooperation can simplify the structure [26, 27].

While considering high efficiency, polarization insensitivity and wide-angle incidence are also indispensable technical indexes in the collection process, and polarization-insensitive and wide-angle metasurface energy harvesters are better adapted to energy harvesting in real electromagnetic environments.

This paper proposes an integrated metasurface harvester, addressing the aforementioned issues, with polarization-insensitive and wide-angle characteristics. The matching network is eliminated by choosing suitable diodes and unit cell structure, which simplifies the structure and improves the collection efficiency of the device. The three-layer, sandwich-like structure takes into account both structural complexity and manufacturing cost, which is conducive to large-scale promotion and use.

The paper is organized as follows. In Section 2, the designed metasurface unit cell structure is presented, and its performance

* Corresponding author: Hongmei Zhao (zhhm@zzuli.edu.cn).

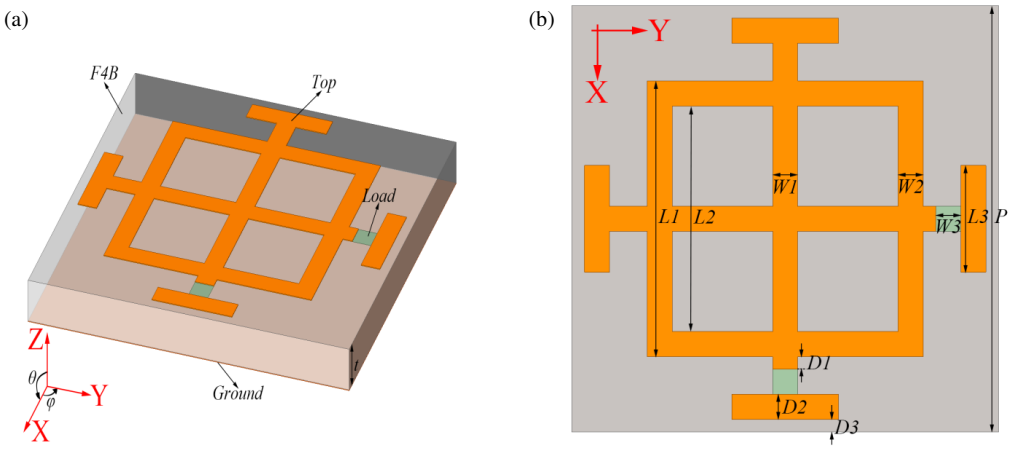

FIGURE 1. Schematic of the metasurface unit cell: (a) 3D view; (b) top view.

is analyzed from multiple perspectives. In Section 3, based on the proposed metasurface structure, the fabrication of the metasurface arrays and the soldering of the devices are carried out for experiments to verify their practical performance and compared with prior literature. In Section 4, the work of this paper is summarized.

2. METASURFACE UNIT CELL DESIGN AND ANALYSIS

The metasurface absorber proposed in this paper consists of a combination of four square patches, two orthogonal dipoles, and a square resonant ring, with a feed gap created by removing two square patches from the orthogonal dipoles to enable easy energy harvesting. The unit cell of the structure is characterized by a standard three-layer configuration, featuring a central dielectric layer made from F4B material (relative permittivity 2.2, dielectric loss tangent 0.0009) with a thickness of $t = 2\,\text{mm}$, with the top resonant structure and bottom ground being etched from 0.035 mm thick copper, as shown in Fig. 1. Resistive loads are placed at the two feed gaps of the orthogonal dipoles to collect the electromagnetic energy captured by the metasurface unit cell. When the resistive loads are replaced with rectifier diodes, DC conversion of the electromagnetic energy can be achieved. The size of the metasurface unit cell is $17\,\text{mm} \times 17\,\text{mm}$, which gives the unit cell perfect energy absorption in the WI-FI band at 5.8 GHz. The length of the square patch is $L3 = 4.5\,\text{mm}$, the width $D2 = 1\,\text{mm}$, the width of the dipole $W1 = 1\,\text{mm}$, the length of the feed-through gap for energy harvesting $W3 = 1\,\text{mm}$, the length of the shorter part of the dipole exposed to the square ring $D1 = 0.5\,\text{mm}$, the outer length of the square ring constituting the unit cell $L1 = 11\,\text{mm}$, the inner length $L2 = 9\,\text{mm}$, and the width of the square ring $W2 = 1\,\text{mm}$. The metasurface unit cell exhibits a symmetric and centrosymmetric structure. The overall size of the resonant unit cell is $16\,\text{mm} \times 16\,\text{mm}$, with a distance from the surrounding boundary $D3 = 0.5\,\text{mm}$, derived from the distance between neighboring unit cells being 1 mm, facilitating uniform coupling between the metasurface unit cells.

The metasurface harvester proposed in this paper is simulated and optimized in the electromagnetic simulation software Ansys HFSS. Two impedances are placed at the two feed gaps of the metasurface harvester to replace the conjugate input impedance of the diode. A Schottky diode HSMS-2860 is used as a rectifier for the metasurface harvester due to its low on-state voltage of 0.28 V and fast switching speed at 5.8 GHz. The metasurface unit cell's geometrical parameters have been carefully tuned for impedance conjugation, ensuring that the output impedance at the feed gap corresponds to the input impedance of the rectifier diode. This optimization is essential for the effective capture and conversion of energy by the metasurface unit cell. Since the input impedance of the diode HSMS-2860 terminated with a $100\,\Omega$ load at 5.8 GHz is $Z = 160 - j28\,\Omega$, the load at the feed gap of the metasurface unit cell is chosen to be a lumped resistor of $Z_d = 160 + j28\,\Omega$, which ensures that the load at the port is conjugate-matched to the input impedance of the diode. Fig. 2 shows the S_{11} and absorption efficiency (RF-AC) of the metasurface unit cell both with and without resistance loading. It is evident that the S_{11} of the metasurface unit cell with resistance loading is significantly reduced, and the absorption efficiency is substantially higher than the unloaded condition. Specifically, the absorption efficiency at 5.8 GHz for the metasurface unit cell without resistance loading is 58.27%, whereas with resistance loading, it reaches 99.87%. In the frequency range of 5.54–6.05 GHz, the S_{11} of the resistor-loaded

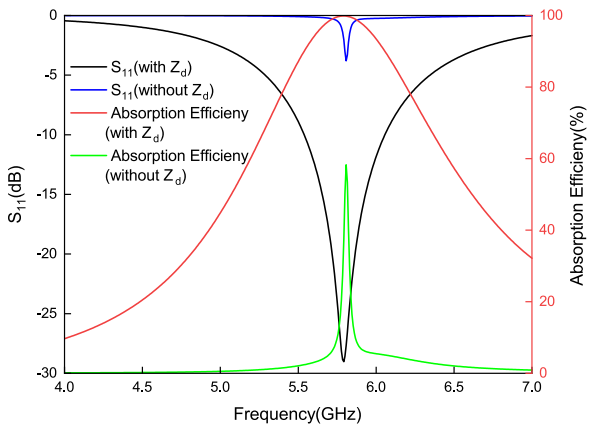

FIGURE 2. S_{11} and absorption efficiency of metasurface unit cell.

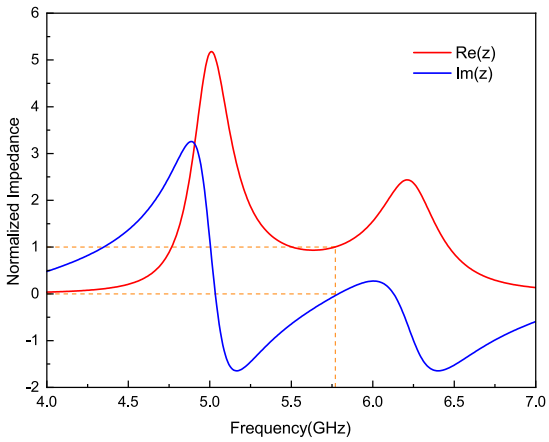

FIGURE 3. Normalized impedance of metasurface unit cell.

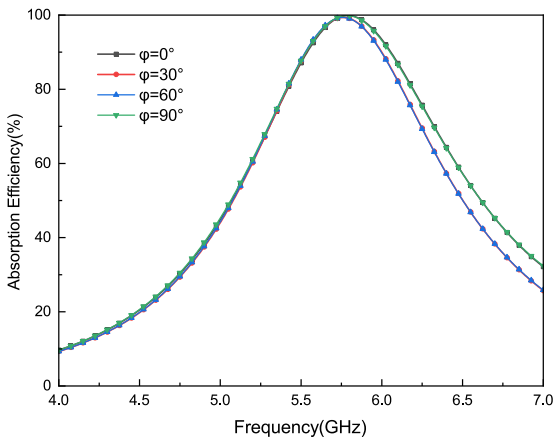

FIGURE 4. Absorption efficiency of metasurface unit cell at different polarization angles.

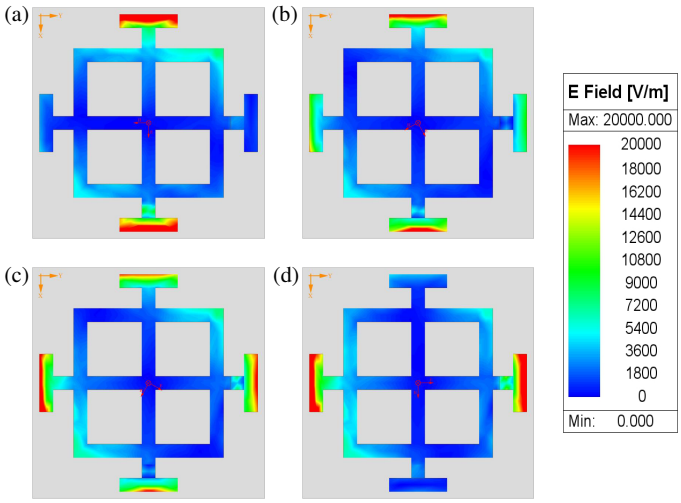

FIGURE 5. The distribution of the electric field within the metasurface unit cell at a frequency of 5.8 GHz is depicted across different polarization angles: (a) $\varphi = 0°$; (b) $\varphi = 30°$; (c) $\varphi = 60°$; (d) $\varphi = 90°$.

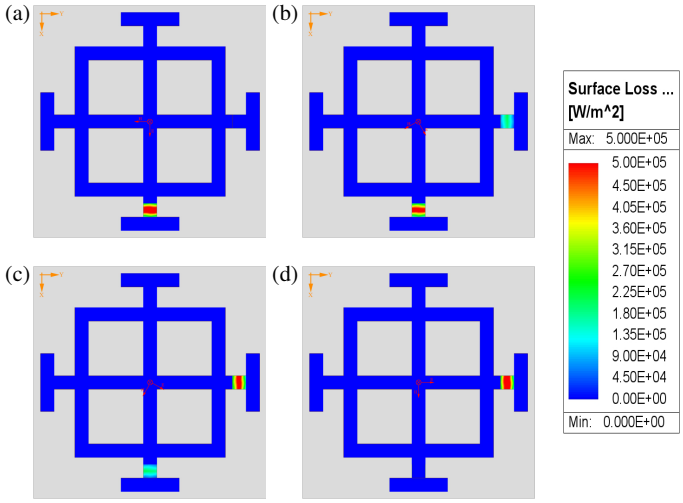

FIGURE 6. The distribution of power loss across the metasurface unit cell at a frequency of 5.8 GHz is characterized for various polarization angles: (a) $\varphi = 0°$; (b) $\varphi = 30°$; (c) $\varphi = 60°$; (d) $\varphi = 90°$.

metasurface unit cell remains below -10 dB, and the range of the S_{11} below -10 dB demonstrates that the metasurface unit cell exhibits excellent impedance matching with the spatial wave impedance, resulting in an absorption efficiency exceeding 90%.

Figure 3 shows the normalized impedance curve of the metasurface unit cell loaded with $Z_d = 160 + j28\,\Omega$. It can be seen that the normalized impedance of the metasurface unit cell at 5.8 GHz is close to 1 in the real part and 0 in the imaginary part, indicating that the input impedance of the unit cell matches the free space, and the incident electromagnetic wave is almost completely absorbed, with no reflections or scattering present.

In addition, the energy harvesting performance of the metasurface unit cell was analyzed at different polarization angles. Fig. 4 shows the energy absorption efficiency of the metasurface unit cell across various polarization angles, specifically at $\varphi = 0°$, $\varphi = 30°$, $\varphi = 60°$, and $\varphi = 90°$. The electromagnetic energy collected on the metasurface unit cell is the sum of the energy collected by the load in the X and Y directions. The simulation outcomes reveal that the metasurface unit cell maintains a stable and uniformly high energy collection efficiency across different polarization angles, specifically at $\varphi = 0°$, $\varphi = 30°$, $\varphi = 60°$, and $\varphi = 90°$. Notably, at a frequency of 5.8 GHz, the unit cell achieves an energy collection efficiency of 99.8%. The simulation results demonstrate the polarization-insensitive nature of the metasurface unit cell.

To gain a more explicit comprehension of the energy absorption dynamics within the metasurface unit cell, an analysis of the electric field and power loss distributions at 5.8 GHz was conducted for the metasurface unit cell under various polarizations of the incident electromagnetic wave. Fig. 5 shows the distribution of the electric field within the metasurface unit cell when it is exposed to incident electromagnetic waves with polarization angles of $\varphi = 0°$, $\varphi = 30°$, $\varphi = 60°$, and $\varphi = 90°$. From Fig. 5(a) and Fig. 5(d), it can be seen that the electric field of the metasurface unit cell under the polarization of the incident electric field at $\varphi = 0°$ and $\varphi = 90°$ is mainly concentrated in the part along the direction of the incident electric

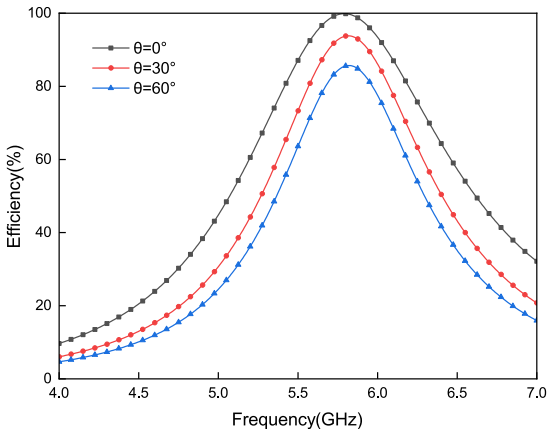

FIGURE 7. Absorption efficiency of metasurface unit cell at different incidence angles.

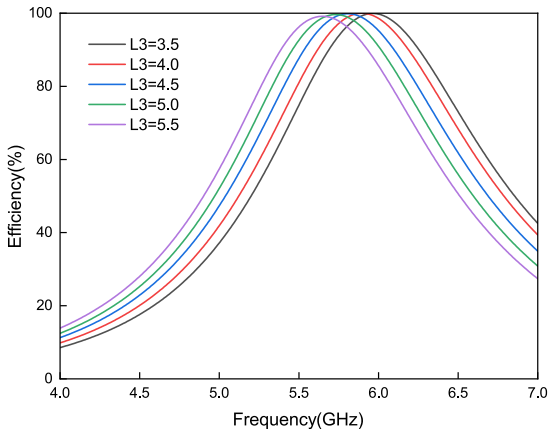

FIGURE 8. Effect of rectangular patch length $L3$ on absorption performance.

field. For polarized incidence at other angles, the incident electric field can be split into vertical and horizontal incident electric field components, and thus the electric field at the surface of the cell is distributed at both feed gaps, as shown in Fig. 5(b) and Fig. 5(c).

Figure 6 shows the distribution of power loss within the metasurface unit cell for incident electromagnetic waves with polarization angles of $\varphi = 0°$, $\varphi = 30°$, $\varphi = 60°$, and $\varphi = 90°$. Upon observation, it is evident that the power loss within the metasurface unit cell, when the incident electric field is polarized at $\varphi = 0°$, is predominantly concentrated along the X-axis feed, aligning with the direction of the electric field. As the polarization angle increases, the power loss along the X-axis feed begins to decrease, while the power loss along the Y-axis feed begins to increase. When the polarization angle increases to 90°, the power loss along the X-axis feed is nearly zero, and at this time, the power loss is completely distributed along the Y-axis feed. This is due to the incident wave's electric field initially having only a vertical component. As the polarization angle changes, the electric field gains both vertical and horizontal components. It is known that only the horizontal component contributes to the power loss.

In actual complex electromagnetic environments, incident waves do not consistently impact the metasurface harvester's surface perpendicularly. Consequently, the absorption performance of the metasurface at various incidence angles, denoted as θ, becomes a critical parameter for assessing the effectiveness of energy harvesting. Fig. 7 shows the absorption efficiency of the metasurface unit cell under TE polarization at varying angles of incidence. Upon examination, it is observed that the metasurface unit cell's absorption at 5.8 GHz experiences a modest decline with an increase in the incidence angle under TE polarization. This is because the intensity of the vertical component of the electromagnetic wave decreases with oblique illumination of the electromagnetic wave to the surface of the structure, which leads to a decrease in the electromagnetic resonance intensity and a slight decrease in the absorption performance. However, when the angle of incidence is increased to 60°, the absorption rate of the metasurface unit cell can still reach more than 80%, which indicates that the metasurface unit cell can maintain good absorption performance under large angle of electromagnetic wave incidence.

To enhance the comprehension of the metasurface harvester's absorption capabilities, an analysis of the structural unit cell's dimensional parameters was conducted. Fig. 8 shows how changes in the length $L3$ of the square patch affect the absorption performance of the metasurface unit cell. It is evident that an increase in $L3$ results in a nearly constant absorption efficiency. However, there is a gradual decrease in the resonant frequency. Fig. 9 depicts the change in the absorption performance of the metasurface unit cell when the thickness t is varied. When t increases, the absorption efficiency changes significantly; the resonant frequency gradually decreases; and the absorption bandwidth gradually becomes wider. Therefore, a suitable $L3$ and t can be selected according to the actual requirements to achieve the perfect absorption of electromagnetic energy at different resonant frequencies of the structural unit cell.

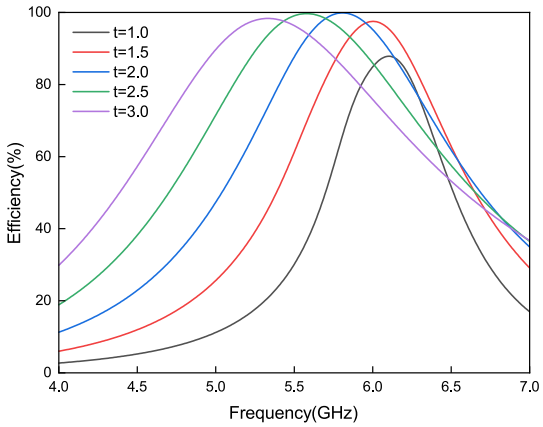

FIGURE 9. Effect of medium thickness t on absorption performance.

3. EXPERIMENTATION AND VERIFICATION

The simulation results indicate that conjugate matching the input impedance of the rectifier diode to the output impedance of the quadrature dipole allows for the elimination of the impedance matching network. Consequently, the direct con-

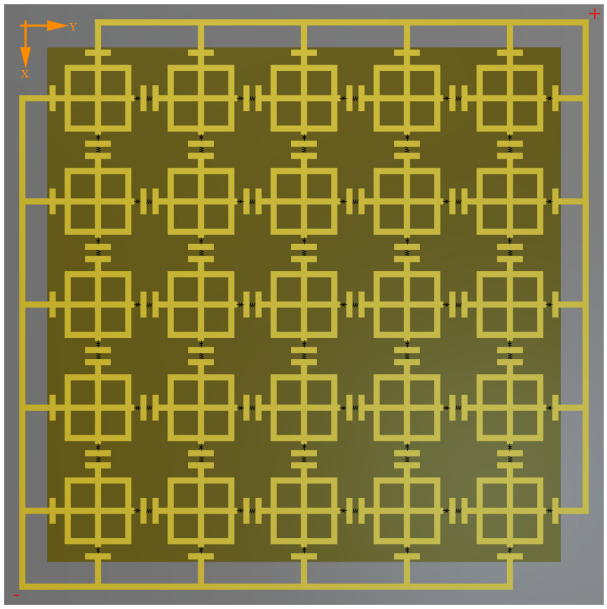

FIGURE 10. Schematic of the DC topology of a 5×5 metasurface harvester.

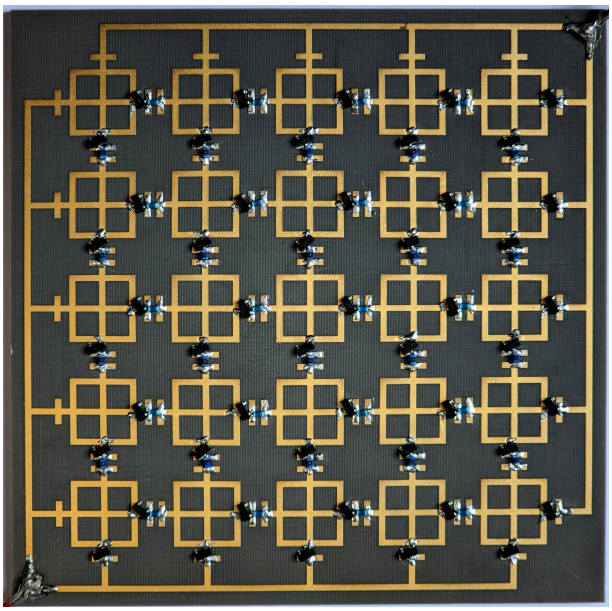

FIGURE 11. Physical metasurface harvester array with integrated diode.

version of radio frequency (RF) energy to direct current (DC) can occur within the metasurface unit cell itself. Next, the matching load at the quadrature dipole feed gap is replaced with a rectifier diode HSMS-2860, and the positive and negative directions of the rectifier diodes are the same in each row and column. On this basis, the neighboring metasurface unit cells are connected by inductors, which not only act as AC filters but also construct DC channels. Therefore, the integrated design of the integrated rectifier diode of the metasurface energy harvester can be realized, and the structural layout of the metasurface energy harvester can be simplified.

Figure 10 shows a schematic topology of the integrated rectified metasurface energy harvester. A 5×5 array of cells is used as an example in the figure, with neighbouring cells connected via inductors. Microstrip lines are used to connect at the end of each row and column to achieve the transmission and aggregation of DC energy in each row and column. As can be seen in Fig. 10, each orthogonal dipole cell rectifies the AC signal by the diode along the X-axis direction when the polarization angle $\varphi = 0°$ of the incident electric field. The cell on each column is connected inductively so that current flows between the cells along the X-axis and is transmitted via microstrip lines at the end of the array to loads at the positive and negative ends of the array. Correspondingly, the power received on the cells on each column is also transferred and pooled at the loads at the end of the array. The diodes along the Y-axis rectify the AC signal with the polarization angle $\varphi = 90°$ of the incident electric field. Similarly, the current on each row circulates between the cells along the Y-axis and is pooled at the end of the array, and the power received on each cell is also pooled along the Y-axis direction to the load at the end of the array. For electric field polarization in the other direction, the two diodes in the orthogonal dipole cell are jointly rectified. The current on the array cells is finally pooled at the end load of the array through the inductors on the X and Y axes, and the power received on the cell is aggregated at the end load of the array. Thus, the design of the integrated diodes in the metasurface array allows for good flow and pooling of energy in each cell, and is not affected by the polarization of the electric field.

A 5×5 metasurface energy harvester was fabricated based on the designed rectified metasurface energy harvester integrated topology, as shown in Fig. 11. The metasurface array was fabricated on a 2 mm thick F4B dielectric substrate, and both the top patch array and bottom metal ground were etched from 35 µm copper. The dimensions of both the top array and bottom metal ground are 85 mm $\times$ 85 mm, and the dimensions of the intermediate dielectric layer, F4B, are 99 mm $\times$ 99 mm, which are larger than the size of the patch array to accommodate the metal wires connecting the structural unit cell in each row and column. Cell gaps in the array are terminated by Schottky diodes Avago HSMS-2860. Adjacent cells are connected by low loss 43 nH inductors to block alternating current and create a direct current path.

Figure 12 shows a schematic diagram of the testing of the metasurface harvester. First, an RF signal was generated by a Keysight signal generator (model E8267D PSG) and transmitted through a power amplifier with a gain of 20 dB to a broadband horn antenna (model JXTXLB-10180-SF) with a gain of 11 dB. Then, the incident wave was irradiated from the horn antenna to the metasurface harvester, which was 50 cm away from the horn antenna. Finally, a multimeter was used to measure the DC voltage across the 100 Ω load. The tests were conducted in laboratory.

The efficiency (η) of the metasurface energy harvester can be determined using the formula that represents the ratio of the harvested direct current (DC) power to the incident radio fre-

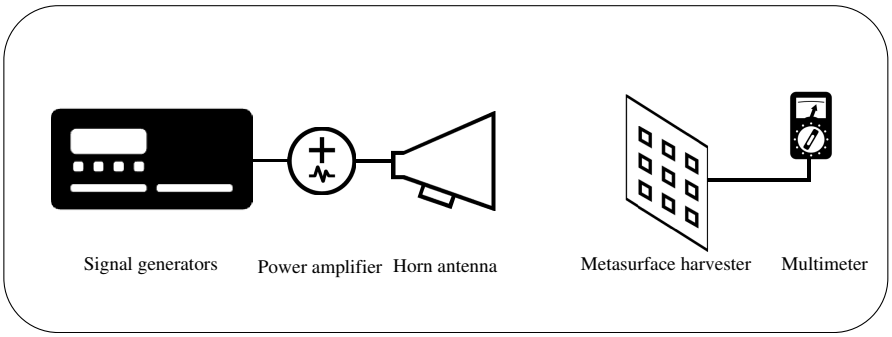

FIGURE 12. Test schematic.

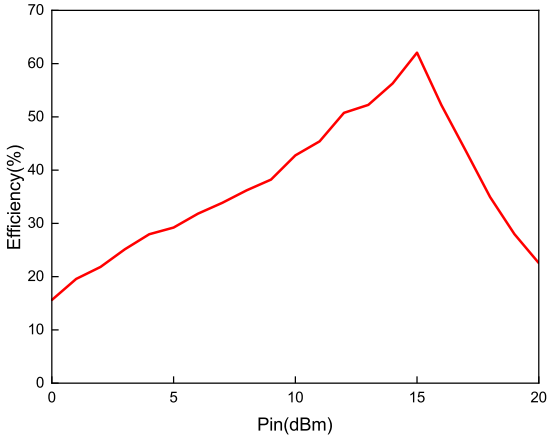

FIGURE 13. Measured efficiency of the harvester at different input powers.

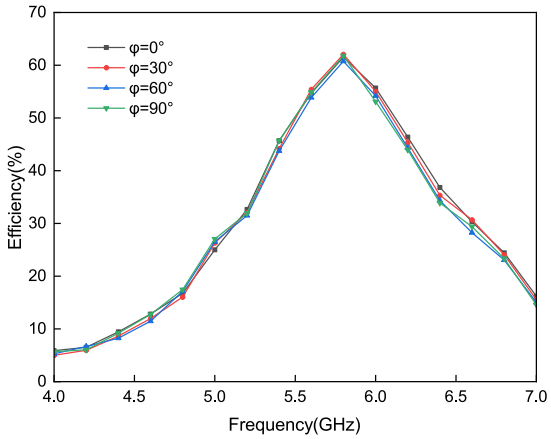

FIGURE 14. Measured efficiency of the harvester at different polarization angles (φ).

quency (RF) power, expressed as:

$$\eta_{\text{meas}} = \frac{P_{dc}}{P_{in}} \times 100\% \tag{1}$$

where P_{dc} is the tributary energy consumed at the load resistance, which can be expressed as:

$$P_{dc} = \frac{V_{out}^2}{R} \tag{2}$$

where V_{out} is the voltage across the load resistor in the rectifier circuit, and R is the load size. P_{in} is the total power incident on the metasurface harvester, denoted as,

$$P_{in} = \frac{G_h \cdot G_p \cdot P_s}{4\pi D^2} \cdot A_{eff} \tag{3}$$

where G_h is the horn antenna gain, G_p the power amplifier gain, P_s the power emitted by the signal generator, D the distance from the horn antenna to the metasurface array, and A_{eff} the effective receiving area of the metarsurface harvester, which is 85 mm $\times$ 85 mm in this paper.

To confirm the accuracy of the simulation outcomes, the actual object underwent testing with respect to several parameters: the power of the incident energy, the angle of polarization, and the angle at which the energy was incident. Firstly, the efficiency of the harvester at 5.8 GHz was tested at different powers, and the results are shown in Fig. 13. It can be seen that the highest energy collection efficiency is achieved at an incident power of 15 dBm. As the power of the incident radiation increases, the efficiency begins to decrease, resulting from the diminishing impedance matching between the metasurface and the diode.

Then, the curves of the efficiency of the metasurface harvester versus polarization angle (φ) were tested at the optimum input power of 15 dBm, and the results are shown in Fig. 14. It can be seen that the curves of the energy collection efficiency of the metasurface versus polarization angle and frequency basically keep the same trend, with only minor fluctuations in efficiency, and the maximum efficiency is about 62.07%. This result has the same characteristics as that of Fig. 4, which verifies that the structure has a polarization-insensitive characteristic. The measured efficiency is lower than the simulated one in Fig. 4. One of the reasons is that the simulated efficiency is the RF to AC efficiency, defined as the ratio of the energy absorbed by the impedance load at the feed gap to the energy irradiated onto the effective area of the metasurface harvester. The measured efficiency is the RF to DC efficiency, defined as the ratio of the energy absorbed by the end resistor after diode rectification to the energy incident on the effective area irradiated to the metasurface harvester. In addition, an infinite periodic array was used for the simulation, whereas a finite 5×5 array was used for the measurement. In conclusion, the designed metasurface harvester is polarization-insensitive and therefore has a wider range of application scenarios.

TABLE 1. Performance comparison of proposed design and related works.

References	Frequency (GHz)	Structure size (mm)	Use of Matching Network	Complexity	Maximum Efficiency (RF-DC)	Polarization Mode
[16]	2.43	$26 \times 26 \times 3.07$	NA	Complex (with through-via)	not applicable	Linear & Wide Angle
[17]	5.3	$15.7 \times 15.7 \times 1.542$	Yes	Complex (with through-via)	not applicable	Linear
[19]	3.4	$18.7 \times 38.4 \times 6.35$	No	Simple (single layer)	76%	Linear
[20]	2.75	$50 \times 50 \times 3.175$	No	Simple (single layer)	60%	Linear
[22]	2.45	$67 \times 74 \times 5.524$	Yes	Complex (three layer)	61%	Linear
This Work	5.8	$17 \times 17 \times 2.07$	No	Simple (single layer)	62.07%	Polarization Insensitive & Wide Angle

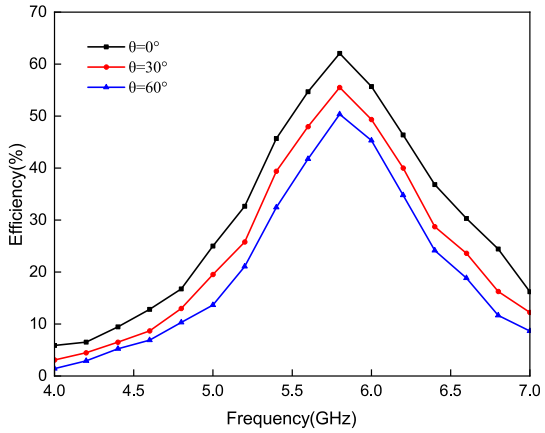

FIGURE 15. Measured efficiency of the harvester at different angles of incidence (θ).

Figure 15 shows the test efficiency of the metasurface harvester as a function of the angle of incidence (θ) when the polarization angle of the incident wave is fixed at 0°. Observably, as the angle of incidence incrementally rises, the efficiency of the harvester experiences a corresponding decline. When the incident wave strikes to the metasurface harvester at a tilt of 60°, the efficiency is still more than 50% at the resonant frequency of 5.8 GHz.

Finally, we compare the metasurface harvester proposed in this paper with previous work. As shown in Table 1, it can be seen that the metasurface harvester proposed in this paper uses only one layer of dielectric substrate, while no through-hole is used. The matching network is eliminated, which reduces the complexity of the structure, and the cell size is smaller, which is favorable for the use in small devices. In addition, while having high efficiency, it also possesses polarization insensitivity and wide-angle characteristics, making it adaptable to varying environmental conditions.

4. CONCLUSIONS

In this paper, a structurally novel and simple integrated rectified metasurface array with polarization-insensitive properties as well as wide-angle characteristics is presented. The complexity of the structure is simplified through extensive analysis, simulation, and testing by using diodes loaded at the openings to eliminate the matching network. In addition, high RF-DC conversion efficiencies can be achieved in the operating frequency band when polarized waves of different polarization modes are incident at different incidence angles. The proposed metasurface harvester has the advantages of small size and low fabrication cost.

REFERENCES

[1] Zanella, A., N. Bui, A. Castellani, L. Vangelista, and M. Zorzi, "Internet of things for smart cities," *IEEE Internet of Things Journal*, Vol. 1, No. 1, 22–32, 2014.

[2] Yu, F., X.-X. Yang, Z. Yi, and S. Gao, "Miniaturized polarization-insensitive rectifying metasurface for powering internet of things devices," *IEEE Antennas and Wireless Propagation Letters*, Vol. 22, No. 7, 1637–1641, 2023.

[3] Chen, D., X. Zhang, W. Zhang, and X. Yin, "Integrated node infrastructure for future smart city sensing and response," *Remote Sensing*, Vol. 15, No. 14, 3699, 2023.

[4] Guo, L., H. Fang, X. Li, W. Yang, and K. Wu, "A rectenna design with quasi-full spatial coverage based on compact dielectric resonator antenna," *IEEE Transactions on Antennas and Propagation*, Vol. 71, No. 10, 7870–7880, 2023.

[5] Elhebeary, M. R., M. A. A. Ibrahim, M. M. Aboudina, and A. N. Mohieldin, "Dual-source self-start high-efficiency microscale smart energy harvesting system for IoT," *IEEE Transactions on Industrial Electronics*, Vol. 65, No. 1, 342–351, 2017.

[6] Sang, J., L. Qian, M. Li, J. Wang, and Z. Zhu, "A wideband and high-gain circularly polarized antenna array for radio-frequency energy harvesting applications," *IEEE Transactions on Antennas and Propagation*, Vol. 71, No. 6, 4874–4887, 2023.

[7] Holloway, C. L., E. F. Kuester, J. A. Gordon, J. O'Hara, J. Booth, and D. R. Smith, "An overview of the theory and applications of

metasurfaces: The two-dimensional equivalents of metamaterials," *IEEE Antennas and Propagation Magazine*, Vol. 54, No. 2, 10–35, 2012.

[8] Shan, D., H. Wang, K. Cao, and J. Zhang, "Wireless power transfer system with enhanced efficiency by using frequency reconfigurable metamaterial," *Scientific Reports*, Vol. 12, No. 1, 331, 2022.

[9] Rong, C., C. Lu, Y. Zeng, X. Tao, X. Liu, R. Liu, X. He, and M. Liu, "A critical review of metamaterial in wireless power transfer system," *IET Power Electronics*, Vol. 14, No. 9, 1541–1559, 2021.

[10] Alemaryeen, A., "Compact wideband antenna for wireless capsule endoscopy system," *Applied Physics A*, Vol. 127, No. 4, 271, 2021.

[11] Jo, S., W. Lee, and H. Lee, "Metasurface patch for wireless power transfer in implantable devices," *Advanced Functional Materials*, Vol. 33, No. 38, 2300027, 2023.

[12] Zhang, H., Y. Li, W. Hu, Q. Lu, B. Zhang, and L. Y. Yang, "Polarization-insensitive electromagnetic metamaterial design for multi-band energy harvesting," *IEEE Access*, Vol. 11, 143 956–143 963, 2023.

[13] Zhang, P., L. Li, X. Zhang, H. Liu, and Y. Shi, "Design, measurement and analysis of near-field focusing reflective metasurface for dual-polarization and multi-focus wireless power transfer," *IEEE Access*, Vol. 7, 110 387–110 399, 2019.

[14] Arrawatia, M., M. S. Baghini, and G. Kumar, "Broadband bent triangular omnidirectional antenna for RF energy harvesting," *IEEE Antennas and Wireless Propagation Letters*, Vol. 15, 36–39, 2015.

[15] Erkmen, F., T. S. Almoneef, and O. M. Ramahi, "Electromagnetic energy harvesting using full-wave rectification," *IEEE Transactions on Microwave Theory and Techniques*, Vol. 65, No. 5, 1843–1851, 2017.

[16] Wagih, M. and S. Beeby, "Thin flexible RF energy harvesting rectenna surface with a large effective aperture for sub $\mu W/cm^2$ powering of wireless sensor nodes," *IEEE Transactions on Microwave Theory and Techniques*, Vol. 70, No. 9, 4328–4338, 2022.

[17] Wei, Y., H. Jing, H. Deng, C. Song, J. Duan, J. Wang, Z. Qu, and B. Zhang, "A dual-band, polarization-insensitive, wide-angle metasurface array for electromagnetic energy harvesting and wireless power transfer," *Results in Physics*, Vol. 46, 106261, 2023.

[18] Erkmen, F. and O. M. Ramahi, "A scalable, dual-polarized absorber surface for electromagnetic energy harvesting and wireless power transfer," *IEEE Transactions on Microwave Theory and Techniques*, Vol. 69, No. 9, 4021–4028, 2021.

[19] Lee, K. and S. K. Hong, "Rectifying metasurface with high efficiency at low power for 2.45 GHz band," *IEEE Antennas and Wireless Propagation Letters*, Vol. 19, No. 12, 2216–2220, 2020.

[20] Liu, N., X. Liu, X. Sheng, X. Li, and H. Ding, "A dual-polarized, notched electromagnetic energy harvester array based on FSS," *IEEE Antennas and Wireless Propagation Letters*, Vol. 23, No. 11, 3782–3786, 2024.

[21] Amer, A. A. G., N. Othman, S. Z. Sapuan, A. Alphones, and A. A. Salem, "High-efficiency electromagnetic energy harvesting using double-elliptical metasurface resonators," *Plos One*, Vol. 18, No. 12, e0291354, 2023.

[22] Duan, X., X. Chen, and L. Zhou, "A metamaterial electromagnetic energy rectifying surface with high harvesting efficiency," *AIP Advances*, Vol. 6, No. 12, 125020, 2016.

[23] He, Z.-J., L.-L. Qiu, P. Zhang, Y. Liu, S. Huang, and L. Deng, "A high-efficiency rectifying metasurface with four operating bands," *IEEE Antennas and Wireless Propagation Letters*, Vol. 22, No. 10, 2387–2391, 2023.

[24] Ashoor, A. Z., T. S. Almoneef, and O. M. Ramahi, "A planar dipole array surface for electromagnetic energy harvesting and wireless power transfer," *IEEE Transactions on Microwave Theory and Techniques*, Vol. 66, No. 3, 1553–1560, 2017.

[25] Almoneef, T. S., F. Erkmen, M. A. Alotaibi, and O. M. Ramahi, "A new approach to microwave rectennas using tightly coupled antennas," *IEEE Transactions on Antennas and Propagation*, Vol. 66, No. 4, 1714–1724, 2018.

[26] Li, L., X. Zhang, C. Song, W. Zhang, T. Jia, and Y. Huang, "Compact dual-band, wide-angle, polarization-angle-independent rectifying metasurface for ambient energy harvesting and wireless power transfer," *IEEE Transactions on Microwave Theory and Techniques*, Vol. 69, No. 3, 1518–1528, 2020.

[27] Ashoor, A. Z. and O. M. Ramahi, "Polarization-independent cross-dipole energy harvesting surface," *IEEE Transactions on Microwave Theory and Techniques*, Vol. 67, No. 3, 1130–1137, 2019.